

Ultrafast switching of telecom photon-number states

Kate L. Fenwick,¹ Frédéric Bouchard,^{1,*} Alicia Sit,¹ Timothy Lee,² Andrew H. Proppe,^{1,2} Guillaume Thekkadath,¹ Duncan England,¹ Philip J. Bustard,¹ Jeff S. Lundeen,² and Benjamin J. Sussman^{1,2}

¹*National Research Council of Canada, 100 Sussex Drive, Ottawa, Ontario K1A 0R6, Canada*

²*Department of Physics, University of Ottawa, Advanced Research Complex,
25 Templeton Street, Ottawa ON Canada, K1N 6N5*

A crucial component of photonic quantum information processing platforms is the ability to modulate, route, convert, and switch quantum states of light noiselessly with low insertion loss. For instance, a high-speed, low-loss optical switch is crucial for scaling quantum photonic systems that rely on measurement-based feed-forward approaches. Here, we demonstrate ultrafast all-optical switching of heralded photon-number states using the optical Kerr effect in a single-mode fiber. A local birefringence is created by a high-intensity pump pulse at a center wavelength of 1030 nm that temporally overlaps with the 1550 nm photon-number states in the fiber. By taking advantage of the dispersion profile of commercially available single-mode fibers, we achieve all-optical switching of photon-number states, with up to 6 photons, with a switching resolution of 2.3 ps. A switching efficiency of >99% is reached with a signal-to-noise ratio of 32,000.

The ability to modulate optical signals at high speeds has been a foundational technology in the telecommunications industry and a cornerstone of fundamental research in atomic, molecular, and optical physics. As we enter the next era of quantum photonic technologies, the design and implementation of fast optical modulators for single photons and quantum states of light will become increasingly crucial [1–5]. These new tools for quantum photonics will demand far more stringent specifications due to the significant impact that loss and noise can have on the performance of quantum applications. One key area of advancement lies in the development of single-photon modulators and switches capable of operating at speeds achievable only with fully optical control [6–8]. In media with a third-order optical nonlinearity, all-optical switching leverages the high peak intensity of short pulses of light or long propagation length of optical fibers to access the nonlinear properties of a medium, through which a secondary pulse propagates. The nonlinearity is induced at the speed of the response of the electrons in the material, which is much faster than current electronics. While gigahertz-frequency (nanosecond timescale) modulation is routine with electro-optic devices and fast electronics, the terahertz (picosecond timescale) regime remains accessible only through all-optical means at present. Pushing the capabilities of all-optical switching in the ultrafast regime resulting in switching times ranging from hundred femtoseconds to a few picoseconds, has resulted in many applications in ultrafast quantum information processing [9–12].

Quantum technologies have reached a stage where scaling has become the primary challenge in their development and deployment. In photonic platforms, this challenge manifests in two key ways: first, the need to generate and detect quantum states with higher photon numbers or greater squeezing, and second, the ne-

cessity of mitigating loss, which remains a primary limitation in scaling quantum photonic systems [13, 14]. Ultrafast all-optical operation offers novel approaches to addressing the challenges of scaling quantum photonic systems to larger photon-number states. For example, operating at the picosecond timescale enables photon-number-resolving (PNR) capabilities in superconducting nanowire single-photon detectors (SNSPDs) [15, 16]. At these ultrafast timescales, the temporal characteristics of the detector’s output signal provide information about the incident photon number. In contrast, transition-edge sensors (TESs) offer intrinsic PNR capability independent of pulse duration, but their microsecond response time is a significant limitation [17]. By integrating TESs with an ultrafast all-optical switch, their slow operation can be circumvented, enabling fast detection while preserving their superior photon-number resolution.

Beyond detection, a key requirement for scaling quantum photonic systems is the implementation of measurement-based feed-forward operations. Many quantum protocols rely on real-time measurements to conditionally manipulate the remaining quantum state, demanding fast, low-loss switching and modulation. However, the processing of detector signals and subsequent feed-forward to an optical switch introduces latencies on the order of microseconds—timescales over which maintaining coherence in large photonic quantum states becomes increasingly challenging. Ultrafast operation provides a temporal encoding approach known as ultrafast time-bin encoding (UTBE) [12]. At the picosecond timescale, environmental fluctuations are effectively frozen, suppressing decoherence caused by mechanical instabilities and enabling high-fidelity quantum operations. This regime further allows long single-mode fibers to serve as low-loss quantum buffers [18], preserving quantum states while feed-forward operations are executed. The development of high-speed, low-loss all-optical switches and modulators is therefore essential for realizing scalable, real-time adaptive quantum photonic architectures.

* frederic.bouchard@nrc-cnrc.gc.ca

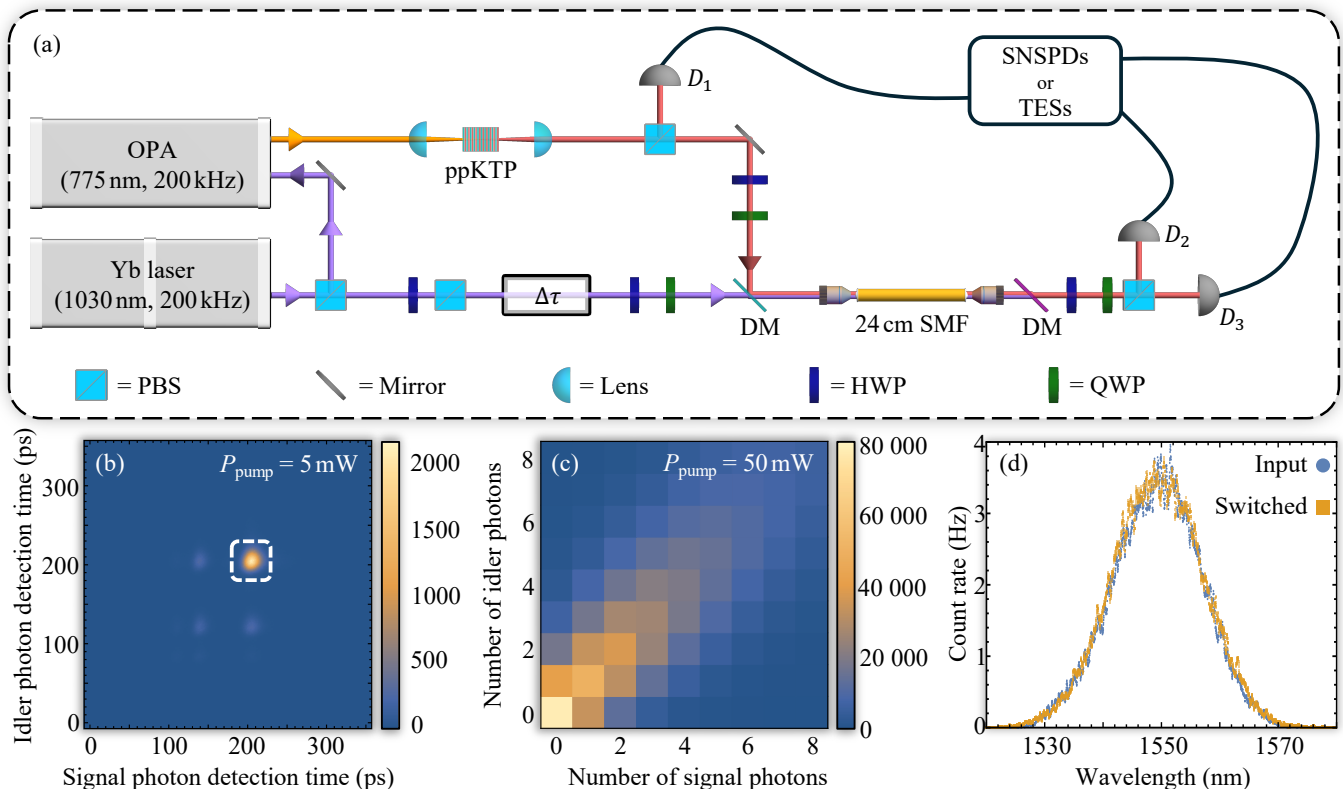


FIG. 1. **Experimental setup.** A simplified experimental setup is shown in (a). Ultrashort pulses at 1030 nm from a 200 kHz Ytterbium (Yb) laser system pump an optical parametric amplifier (OPA) which provides pulses at 775 nm to then pump spontaneous parametric downconversion (SPDC) in a periodically poled potassium titanyl phosphate (ppKTP) crystal for photon-pair generation. The idler photons, measured at detector D_1 , herald the detection of the switched (unswitched) signal photons at detector D_2 (D_3). Signal photons are combined with a portion of the 1030 nm pump beam on a dichroic mirror (DM), after which both beams are launched into the 24 cm single-mode fiber (SMF). Within the SMF, the 1030 nm pump pulses induce the cross-phase modulation (XPM) required to rotate the polarization of the signal photons. A polarizing beamsplitter (PBS) separates the switched and unswitched light, which is detected by either superconducting nanowire single-photon detectors (SNSPDs) or transition-edge sensors (TESs). We extract 2D histograms from the detection events measured by the SNSPDs, as shown in (b), which allow us to filter the one-photon events (enclosed by a white dashed line) from events with more than one photon. We pump the SPDC source with low powers (5 mW) for the single-photon switching demonstrations made with the SNSPDs. On the other hand, the source is pumped with higher power (50 mW) for the heralded switching of number states with up to 6 photons, as measured by the TESs. A joint photon-number intensity measurement is shown in (c) for the high power case. The signal photon spectrum remains unchanged by the switch, as shown in (d). HWP: half-wave plate; QWP: quarter-wave plate; $\Delta\tau$: pump delay line.

Finally, operating in the ultrafast regime expands the quantum photonics toolkit by providing access to broad optical bandwidths. For instance, the large bandwidth of ultrashort pump pulses is leveraged in state-of-the-art heralded single-photon sources to achieve high spectral purity, while their high pulse energy enables stronger squeezing, supporting the generation of large heralded photon-number states [19]. Despite the advantages and promises of ultrafast quantum photonics, most demonstrations of all-optical switching have been concentrated in the visible regime (around 800 nm) [20–22], whereas the telecom band (1550 nm) remains relatively less explored. Evidence of low loss, ultrafast switching of telecom single photons has been reported [23], yet a high-efficiency implementation remains an open challenge, for

which this work presents a solution. Advances in superconducting detection have enabled low-jitter, photon-number-resolving detectors optimized for telecom wavelengths, where optical fiber transmission losses are minimized. As quantum photonic technologies scale, integrating ultrafast all-optical components with these detectors will be important for realizing high-speed, low-loss quantum information processing systems.

In this work, we design and demonstrate a high-efficiency all-optical switch which operates on heralded photon-number states in the telecom band with picosecond resolution, low noise, and low loss. The switch relies on cross-phase modulation (XPM) via the optical Kerr effect in a short single-mode fiber (SMF) [24]. The Kerr effect, a third-order nonlinear process, induces an

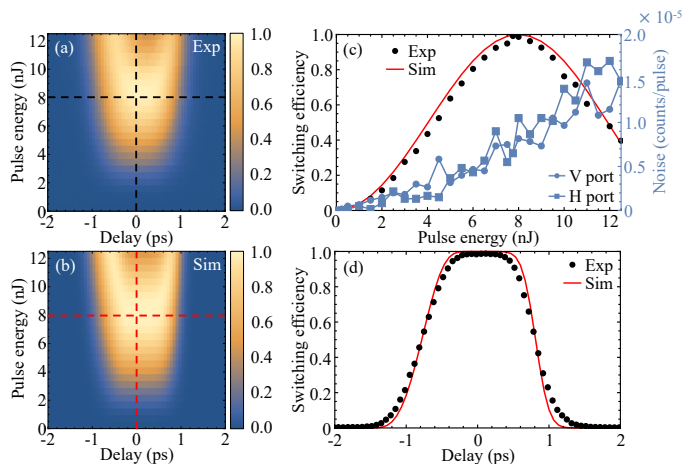


FIG. 2. **Characterizing the switch.** The experimental and simulated switching efficiency, as a function of pump pulse energy and delay, are shown in (a) and (b), respectively. Slices from these 2D datasets are shown for (c) a constant pump pulse delay of $\Delta\tau = 0$ and (d) a constant pump pulse energy of 8 nJ, where the black circles correspond to experimental data and red lines correspond to simulation results. Also shown in (c) are the measured pump noise counts per pulse, indicated by the blue circles and squares for the switched (V) and unswitched (H) ports, respectively. Here, SNSPDs are used for experimental measurements.

intensity-dependent change in the refractive index of the fiber due to the nonlinear polarization response of the material. For example, when a high-intensity pump pulse propagates through the fiber, it induces a local birefringence, altering the refractive index experienced by a co-propagating, weaker signal pulse. This XPM effect can be used to manipulate the polarization of the signal pulse, depending on the pump pulse intensity and polarization. Precise control over the pump pulse intensity, and the relative polarization and timing between the pump and signal pulses, allows for tunable all-optical switching. With access to ultrashort pulses (hundreds-of-femtoseconds in duration) and detectors with photon-number-resolution (PNR) capabilities, picosecond-resolution switching of photon-number states can be achieved.

Shown in Fig. 1(a), the experiment is driven by a commercial Ytterbium-doped ultrafast laser system (Carbide, LightConversion) delivering 180 fs pulses at a center wavelength of 1030 nm with a 200 kHz repetition rate. The beam is split, with the majority directed to an optical parametric amplifier (Orpheus-HP, LightConversion) tuned to 775 nm which pumps a 2 mm type-II periodically poled potassium titanyl phosphate (ppKTP) crystal. Degenerate photon pairs at 1550 nm are generated via spontaneous parametric down-conversion (SPDC), with the signal and idler photons separated by a polarizing beam splitter (PBS). The idler photons are detected (at D_1) to herald the signal photons, which are coupled into a 24 cm SMF (1060XP, Thorlabs) and switched.

Part of the remaining 1030 nm beam is coupled into

this 24 cm SMF to pump the XPM process required for switching. Spatiotemporal overlap between the pump pulse and signal photons is achieved by recombining the beams on a dichroic mirror prior to the SMF, and adjusting their relative delay, $\Delta\tau$. The polarization of the pump pulse is precisely set to maximize the polarization rotation of the signal photons. The temporal resolution of the all-optical switch is determined by two effects: the pulse duration of the pump and the group velocity difference between the pump and signal, caused by dispersion in the fiber. This group velocity walk-off, which broadens the interaction time here to approximately 1 ps, is beneficial as it enables uniform switching across the entire signal photon wavepacket.

After the 24 cm SMF, the 1030 nm pump pulses are spectrally filtered and a PBS splits the switched and unswitched light into two detection channels, D_2 and D_3 , respectively. The measured insertion loss of the switch, which includes all relevant optical components to achieve near-unity switching (see Supplemental Material), is 3 dB. The signal and idler photons are detected with either superconducting nanowire single-photon detectors (SNSPDs) or transition-edge sensors (TESs), where PNR capabilities are accessible in both configurations. The SNSPDs used here have a low jitter time of ~ 20 ps, which can be leveraged to separate one-photon detection events from multi-photon detection events. By operating the SNSPDs with an appropriate trigger level, one-photon events will trigger a detection later than two-photon events, and so on. This can be seen in Fig. 1(b), where the bright spot, circled by the dashed white outline, corresponds to coincidence events in which one photon is measured in both the signal and idler channels. When operating the switch with SNSPDs, we consider only coincidences measured in the window enclosed by the dashed white outline to filter out any detection events arising from more than one heralded photon. It is important to note that the PNR capabilities of the SNSPDs are only accessible when operating on ultrafast timescales, as demonstrated here. The TES detectors, on the other hand, provide photon counting capabilities up to higher photon numbers. The joint photon-number distribution of the source, as measured with TESs, is presented in Fig. 1(c). Note that switching demonstrations with the SNSPDs and TESs were performed by pumping the SPDC process with low (5 mW) and high (50 mW) pump powers, respectively. The joint photon-number intensity distribution was measured over a range of pump powers, included in the Supplemental Material. Importantly, the spectrum of switched photons is not changed by the switching process, as demonstrated in Fig. 1(d). Here, we achieve spectrally resolved detection of the signal photons with a dispersion compensating module (SMFDK-S-060-03-10 from OFS), which has a group delay dispersion of $D = 1033$ ps/nm, and the SNSPDs to implement a time-of-flight spectrometer [25]. The spectrally resolved signal photons are heralded by detection of the idler photon.

In order to assess the performance of our switch, we

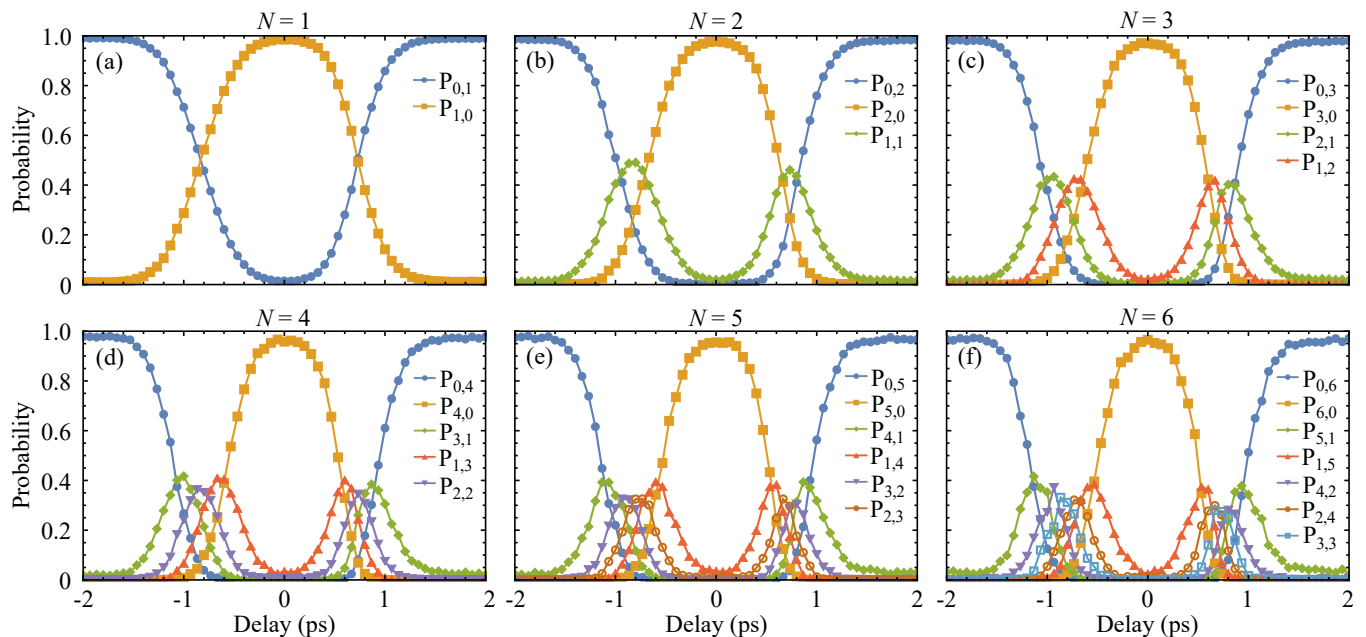


FIG. 3. **Switching of heralded photon-number states.** The measured probability, P_{n_2, n_3} , of measuring n_2 photons at D_2 and n_3 photons at D_3 , heralded by a measurement of N photons at D_1 , where $n_2 + n_3 = N$, is shown in (a)–(f) for $N = 1$ –6. TESs are used for all measurements presented here. Data points are connected by lines to help guide the eye.

calculate its switching efficiency, for which a theoretical description is provided in the Supplemental Material. We first operate the source in the low power regime, measuring coincidence rates between one idler photon and its corresponding switched or unswitched signal photon using the SNSPDs. From these coincidence measurements, we can determine the experimental switching efficiency as

$$\eta_{\text{exp}} = N_{s_V, i} / (N_{s_H, i} + N_{s_V, i}), \quad (1)$$

where $N_{s_H, i}$ and $N_{s_V, i}$ represent the coincidence rates between the idler photon and the signal photon exiting the horizontally (unswitched) and vertically polarized (switched) output ports of the PBS, respectively. The measured switching efficiency is shown in Fig. 2(a), as a function of both pump pulse energy and relative delay between the pump and signal, $\Delta\tau$.

Experimental measurements are compared to a comprehensive simulation, as seen in Fig. 2(b), which uses the split-step Fourier method to solve the generalized pulse propagation equation. We model the evolution of both the strong pump and weak signal photons, based on the dispersion curve provided by the vendor for the 24 cm 1060XP SMF. Further details on the simulation are provided in the Supplemental Material. We first validate our model by comparing the simulated output spectra with the experimentally measured spectra, confirming the expected self-phase-modulation-induced spectral broadening of the pump pulses as a function of their energy. With this validated model, the detailed propagation of the pump and signal photon wavepackets through

the SMF can be simulated, along with the deconvoluted switching response. These simulations provide insight into the dynamics driving the observed switching behavior and allow us to analyze the nonlinear and dispersive effects that influence the switching response.

For a fixed delay of $\Delta\tau = 0$ ps, as seen in Fig. 2(c), the switching efficiency increases with pump pulse energy, following the expected quadratic sinusoidal curve. For a pump pulse energy of 8 nJ, we achieve a switching efficiency of $> 99\%$. Beyond this point, the efficiency decreases, as the nonlinear phase shift induced by the pump exceeds the point at which $\Delta\phi = \pi$. This behaviour is observed in both the experimental data and simulation results, which show good qualitative agreement. Notably, we observe approximately 1×10^{-5} noise counts per pump pulse in each of the signal detection ports (*i.e.*, the horizontally (H) and vertically (V) polarized outputs from the PBS). Given a measured heralding efficiency of 32% for the full switching setup, we can infer a signal-to-noise ratio of 32,000.

An important characteristic of our all-optical switch is its temporal resolution, crucial for enabling ultrafast time-bin encoding [10–12, 22] and other ultrafast quantum photonic applications in the telecom band. The temporal profile of the switch can be seen in Fig. 2(d), where switching efficiency is plotted as a function of delay $\Delta\tau$, for a fixed pump pulse energy of 8 nJ. Again, we see good qualitative agreement between the experimental measurements and simulation results. The switching resolution, determined by considering the full width at 10 dB, is found to be 2.3 ps. Notably, the top of the curve remains flat near 100% switching efficiency, indi-

cating that the switch is insensitive to small variations in pump arrival time within this region. This flatness suggests that the pump pulse has fully traversed the signal photon wavepacket in the SMF, imprinting a nearly uniform temporal phase profile. Such uniformity is essential for achieving near-unity switching efficiency.

Given the high efficiency performance of the switch in the single-photon regime, as measured with the SNSPDs, we next investigate its ability to operate on heralded photon-number states, as measured with TESs. As shown in Figs. 3(a)–(f), we measure $N = 1$ –6 idler photon at D_1 , to herald the detection of $N = 1$ –6 signal photons at the output of the switch, monitoring the probability of each possible outcome, P_{n_2, n_3} , where n_2 and n_3 are the number of photons measured at D_2 and D_3 , respectively. Once again, we observe near-unity switching efficiency at $\Delta\tau = 0$. For $N > 1$, we see peaks in the probabilities for $n_2, n_3 < N$ that are associated with the splitting ratio at the PBS when the photons have not yet been fully polarization-rotated. Furthermore, we observe that the $P_{N,0}$ curve becomes more narrow for larger N , which is indicative of an increasing sensitivity to the switch splitting ratio. Importantly, we still observe a high switching efficiency for $\Delta\tau = 0$ for large N . These results demonstrate the ability of our switch to reliably act on heralded photon-number states, opening the door to continuous-variable encoding schemes in, *e.g.*, quantum information processing with ultrafast time bins. Furthermore, the switching of Fock states is anticipated to allow for the injecting of nongaussianity into photonic quantum circuits [26], a useful capability in the context of quantum information processing. Heralded photon-number states are the next stage in the evolution of photonic quantum states, providing expanded capabilities in comparison to their predecessors (*i.e.*, attenuated coherent states or two-mode squeezed vacuum without PNR) [27–30].

The results presented in this work showcase the vi-

ability of using the optical Kerr effect in SMF for all-optical switching of photon-number states at picosecond timescales in the telecom band. The demonstrated near-unity switching efficiency, combined with minimal insertion loss and low noise levels, underscores the practicality of this approach for ultrafast quantum photonic applications, such as time-bin encoding. Further, the ability to switch heralded-photon number states at these ultrafast timescales opens the door to next-generation quantum technologies which are anticipated to rely on photon number as a resource. The interplay between group velocity mismatch and self-phase modulation in the fiber plays a critical role in shaping the temporal profile of the switch, as supported by both experimental data and numerical simulations. Further refinement to this technique could include enhancing performance by improving polarization control and optimizing fiber dispersion. Investigating alternative fiber geometries or nonlinear media may also lead to greater control over the spectral and temporal characteristics of the switch. This platform represents a promising step toward scalable quantum photonic systems, where precise control over photon-number states on ultrafast timescales will enable advances in quantum communication, computation, and metrology.

ACKNOWLEDGMENTS

We thank Khabat Heshami, Aaron Goldberg, Yingwen Zhang, Ramy Tannous, Nicolas Couture, Noah Lupu-Gladstein, Jonathan Baker, Nicolas Dalbec-Constant, Nathan Roberts, Milica Banic, Denis Guay, Doug Mofatt, and Rune Lausten for support and insightful discussions.

-
- [1] R. Prevedel, P. Walther, F. Tiefenbacher, P. Böhi, R. Kaltenbaek, T. Jennewein, and A. Zeilinger, *Nature* **445**, 65 (2007).
 - [2] M. Miková, H. Fikerová, I. Straka, M. Mičuda, J. Fiurášek, M. Ježek, and M. Dušek, *Physical Review A—Atomic, Molecular, and Optical Physics* **85**, 012305 (2012).
 - [3] I. Shomroni, S. Rosenblum, Y. Lovsky, O. Bechler, G. Guendelman, and B. Dayan, *Science* **345**, 903 (2014).
 - [4] F. Kaneda and P. G. Kwiat, *Science advances* **5**, eaaw8586 (2019).
 - [5] E. Meyer-Scott, N. Prasanna, I. Dhand, C. Eigner, V. Quiring, S. Barkhofen, B. Brecht, M. B. Plenio, and C. Silberhorn, *Physical Review Letters* **129**, 150501 (2022).
 - [6] M. A. Hall, J. B. Altepeter, and P. Kumar, *Physical review letters* **106**, 053901 (2011).
 - [7] M. A. Hall, J. B. Altepeter, and P. Kumar, *New Journal of Physics* **13**, 105004 (2011).
 - [8] C. Kupchak, J. Erskine, D. England, and B. Sussman, *Optics letters* **44**, 1427 (2019).
 - [9] F. Bouchard, D. England, P. J. Bustard, K. L. Fenwick, E. Karimi, K. Heshami, and B. Sussman, *Physical Review Applied* **15**, 024027 (2021).
 - [10] F. Bouchard, D. England, P. J. Bustard, K. Heshami, and B. Sussman, *PRX Quantum* **3**, 010332 (2022).
 - [11] K. L. Fenwick, F. Bouchard, G. S. Thekkadath, D. England, P. J. Bustard, K. Heshami, and B. Sussman, *Optica* **11**, 1017 (2024).
 - [12] F. Bouchard, K. Fenwick, K. Bonsma-Fisher, D. England, P. J. Bustard, K. Heshami, and B. Sussman, *Phys. Rev. Lett.* **133**, 090601 (2024).
 - [13] H. Aghaee Rad, T. Ainsworth, R. Alexander, B. Altieri, M. Askarani, R. Baby, L. Banchi, B. Baragiola, J. Bourassa, R. Chadwick, *et al.*, *Nature*, 1 (2025).
 - [14] *Nature*, 1 (2025).
 - [15] C. Cahall, K. L. Nicolich, N. T. Islam, G. P. Lafyatis, A. J. Miller, D. J. Gauthier, and J. Kim, *Optica* **4**, 1534

- (2017).
- [16] D. Zhu, M. Colangelo, C. Chen, B. A. Korzh, F. N. Wong, M. D. Shaw, and K. K. Berggren, *Nano Letters* **20**, 3858 (2020).
- [17] T. Gerrits, A. Lita, B. Calkins, and S. W. Nam, *Superconducting devices in quantum optics*, 31 (2016).
- [18] K. F. Lee, G. Gül, Z. Jim, and P. Kumar, *New Journal of Physics* **26**, 083011 (2024).
- [19] G. Harder, T. J. Bartley, A. E. Lita, S. W. Nam, T. Gerrits, and C. Silberhorn, *Physical review letters* **116**, 143601 (2016).
- [20] J. M. Donohue, M. Agnew, J. Lavoie, and K. J. Resch, *Physical Review Letters* **111**, 153602 (2013).
- [21] C. Kupchak, P. J. Bustard, K. Heshami, J. Erskine, M. Spanner, D. G. England, and B. J. Sussman, *Physical Review A* **96**, 053812 (2017).
- [22] F. Bouchard, K. Bonsma-Fisher, K. Heshami, P. J. Bustard, D. England, and B. Sussman, *Physical Review A* **107**, 022618 (2023).
- [23] U. Purakayastha, C. P. Lualdi, and P. G. Kwiat, in *Frontiers in Optics* (Optica Publishing Group, 2022) pp. FTu6B–1.
- [24] D. England, F. Bouchard, K. Fenwick, K. Bonsma-Fisher, Y. Zhang, P. J. Bustard, and B. J. Sussman, *Applied Physics Letters* **119**, 160501 (2021).
- [25] M. Avenhaus, A. Eckstein, P. J. Mosley, and C. Silberhorn, *Optics letters* **34**, 2873 (2009).
- [26] V. Crescimanna, A. Z. Goldberg, and K. Heshami, *Physical Review A* **109**, 023717 (2024).
- [27] I. Afek, O. Ambar, and Y. Silberberg, *Science* **328**, 879 (2010).
- [28] S. Konno, W. Asavanant, F. Hanamura, H. Nagayoshi, K. Fukui, A. Sakaguchi, R. Ide, F. China, M. Yabuno, S. Miki, *et al.*, *Science* **383**, 289 (2024).
- [29] K. Takase, J.-i. Yoshikawa, W. Asavanant, M. Endo, and A. Furusawa, *Physical Review A* **103**, 013710 (2021).
- [30] M. Endo, T. Nomura, T. Sonoyama, K. Takahashi, S. Takasu, D. Fukuda, T. Kashiwazaki, A. Inoue, T. Umeki, R. Nehra, *et al.*, arXiv preprint arXiv:2502.08952 (2025).